

TWENTY FIRST EUROPEAN ROTORCRAFT FORUM

Paper No VI-3

**INVESTIGATION OF DYNAMIC INFLOW'S INFLUENCE
ON ISOLATED ROTOR FLAP/LAG STABILITY
AND COUPLED ROTOR/BODY STABILITY**

Jinsong Bao

**Research Institute of Helicopter Technology
Nanjing University of Aeronautics and Astronautics
Nanjing, CHINA**

Xiaogu Zhang

**Department of Aircraft Design and Applied Mechanics
Beijing University of Aeronautics and Astronautics
Beijing, CHINA**

**August 30-September 1, 1995
SAINT-PETERSBURG, RUSSIA**

Paper nr.: VI.3

Investigation of Dynamic Inflow's Influence on Isolated Rotor Flap/Lag
Stability and Coupled Rotor/Body Stability.

Jinsong Bao; Xiaogu Zhang

TWENTY FIRST EUROPEAN ROTORCRAFT FORUM

August 30 - September 1, 1995 Saint-Petersburg, Russia

Investigation of Dynamic Inflow's Influence on
Isolated Rotor Flap/Lag Stability and Coupled Rotor/Body Stability

Jinsong Bao

Research Institute of Helicopter Technology
Nanjing University of Aeronautics and Astronautics
Nanjing 210016. CHINA

Xiaogu Zhang

Department of Aircraft Design and Applied Mechanics
Beijing University of Aeronautics and Astronautics
Beijing 100083. CHINA

Abstract

Dynamic inflow model is a relatively simple inflow model for the unsteady aerodynamics. A method taking dynamic inflow into account is developed to analyse the rotor flap/lag stability and coupled rotor/body stability in hover. The analytical model is verified through the comparative study between theoretical results and experimental data. The correlation between the theoretical and measured data is excellent. The sensitivity of the results to difference in dynamic inflow model L matrix is also examined. The influence of dynamic inflow in different uncoupled dimensionless blade flap and lead-lag natural frequency and rotor speed is investigated. The parameters used in the analysis are typical for conventional hingeless rotor helicopters. The inflow mode is carefully identified. Through the analysis of the mutual excitation and the analysis of mode shapes, the effect of inflow mode on the stability is studied.

I_h	ratio of the average value of helicopter roll and pitch inertia to rotor roll or pitch inertia
v	perturbated induced inflow
v_0, v_s, v_c	mean, lateral and longitudinal components of perturbated induced inflow
α	blade angle of attack
β_c, β_s	longitudinal and lateral rotor disc-plane tilt
γ	blade Lock number
δI_h	nonidentity of helicopter pitch and roll inertia
θ_0	blade collective pitch angle
ξ_c, ξ_s	lateral and longitudinal rotor lead-lag motion
ξ_k	perturbation lead-lag motion of the kth blade
ξ_0	equilibrium lag angle
σ	real part of eigenvalue; modal damping; rotor solidity
φ_x, φ_y	body roll and pitch motion
Ω	rotor angular velocity
Ω_0	rotor normal speed
ψ_k	azimuth angle of the kth blade
ω	imaginary part of eigenvalue; modal frequency
ω_s, ω_l	uncoupled fundamental flap and lead-lag frequencies
()	()/R; ()/ Ω
(')	d()/d φ

Notation

C_d	blade profile drag coefficient
C_l	blade profile lift coefficient
C_A	rotor aerodynamic load coefficients
h	distance from body C. G. to rotor plane
r	distance from rotor center
R	rotor radius

Introduction

Unsteady aerodynamics has a significant influence on the isolated rotor flap/lag stability and coupled rotor/body stability characteristics. It is important to set up practical unsteady aerodynamic model. Dynamic inflow is an effective and simple model to deal with unsteady aerodynamics in rotor dynamics. Recently, a method taking dynamic inflow into account was developed to analyse the rotor force and moment, and a dynamic inflow model was verified through the comparative study between analytical results and test data in hover (Ref. 1).

In Ref. 2 and Ref. 3, the influence of various unsteady aerodynamic models on the aeromechanical stability of a helicopter in ground resonance and air resonance was investigated. There seems to have some contradictory results in Refs. 2-3. So, further work has to be done.

In Ref. 4, helicopter air resonance in hover was investigated by complex coordinates. Through the analysis of the approximate expressions of the mutual excitation and the analysis of mode shapes, the physical explanation and the influence of important design parameters on the instability were studied. But the structural model was simple. The unsteady inflow was not taken into account in the analytical model.

In this study, the dynamic inflow is introduced in the investigation of helicopter air resonance. Following Ref. 4, the complex coordinates system is used. An offset-hinged rigid blade is used in the analytical model. The structural coupling between flap and lead-lag motion is also considered. The modes is identified by examining the percentage of different degrees of freedom (d. o. f.). The theoretical results are compared with the experimental data in Ref. 5 and Ref. 6. Then, the influence of dynamic inflow on isolated rotor flap /lag stability and coupled rotor/body stability in different dimensionless flap and lead-lag natural frequency, rotor speed and collective pitch in hover is further

studied. The work done by inflow on other d. o. f. is investigated to give the physical explanation of the effect of dynamic inflow.

Dynamic Inflow Model

The theory of dynamic inflow is the mathematical modeling of induced flow response to variations in rotor aerodynamic loads. Dynamic inflow is viewed globally as rotor disk downwash dynamics under unsteady conditions. In dynamic inflow model, induced flow perturbation parameters are related with aerodynamic loads by means of ordinary differential equations:

$$M\dot{v} + L^{-1}v = C_A \quad (1)$$

v is the perturbed induced flow. C_A represents the rotor thrust, roll and pitch hub moment coefficients. It is only the aerodynamic component. The matrix L is the static transfer matrix between induced flow and aerodynamic loads. The matrix M reflects the effect of the inertia of air mass, it indicates the delay characteristics of the inflow.

If the v is approximated by a first harmonic Fourier series:

$$v(r, \psi) = v_0 + v_s r \sin \psi + v_c r \cos \psi \quad (2)$$

The M and L can be derived from unsteady actuated disk theory (Ref. 7) in hover.

$$L1 = \frac{1}{2V_s} \begin{bmatrix} 0.5 & 0 & 0 \\ 0 & -2 & 0 \\ 0 & 0 & -2 \end{bmatrix} \quad (3)$$

$$M = \begin{bmatrix} \frac{8}{3\pi} & 0 & 0 \\ 0 & \frac{-16}{45\pi} & 0 \\ 0 & 0 & \frac{-16}{45\pi} \end{bmatrix} \quad (4)$$

In Ref. 8, another L matrix is provided:

$$L_2 = \frac{1}{V_s} \begin{bmatrix} 0.5 & 0 & 0 \\ 0 & -2 & 0 \\ 0 & 0 & -2 \end{bmatrix} \quad (5)$$

In Ref. 2, comparison study between the theoretical results and test data of rotor control derivatives indicates that the results calculated with the L_2 are better matched with test data than those with the matrix L_1 . Therefore the L_2 matrix is used in the analytical model. However, in some cases, the calculation with L_1 is also compared.

Analytical Model

The analytical model shown in Fig. 1 is developed from the basic model described in Ref. 4.

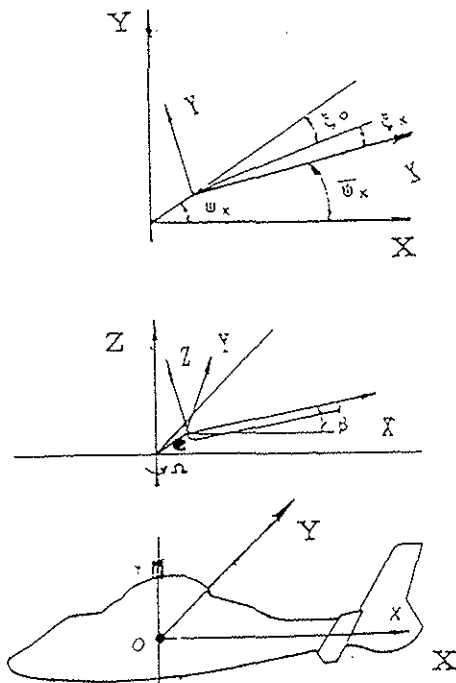


Fig. 1 Analytical model

An offset-hinged rigid blade model is used, with flap and lead-lag spring restraints at the hinge. The blade is assumed to be untwisted and of constant chord and uniform mass distribution. The structural coupling between flap and lead-lag motion is involved in the analytical model. Only rigid fuselage pitch and roll rotation are taken into ac-

count.

The simple strip theory is used to obtain the elemental aerodynamic loads. The section lift and drag coefficient (C_l , C_d) is expressed by following equations.

$$C_l = a_0 + a\alpha \quad (6)$$

$$C_d = C_{x0} + C_{x2}\alpha^2 \quad (7)$$

Eqs. 6-7 can be used to deal with the unsymmetrical airfoil. In Ref. 6, the blade airfoil NACA23012 provides:

$$C_l = 0.15 + 5.73\alpha \quad (8)$$

$$C_d = 0.0079 + 1.7\alpha^2 \quad (9)$$

Dynamic inflow is taken into account in the perturbation equations. Since the uniform component of inflow v_0 does not couple with the cyclic mode, it is not considered in the analysis of the stability.

The individual blade flap and lead-lag motions are combined together and transferred to the fixed system through multiblade coordinate transformation. The flap, lead-lag, body freedoms and dynamic inflow are each combined into one complex variable.

$$\begin{cases} \beta = \beta_c + i\beta_s \\ \xi = \xi_c + i\xi_s \\ v = v_c + iv_s \\ \varphi = \varphi_x + i\varphi_y \end{cases} \quad (10)$$

The β_c, β_s are equivalent to the longitudinal and lateral rotor disc-plane tilt and ξ_c, ξ_s represent the lateral and longitudinal rotor lead-lag motion. The equations of motion are derived by Newtonian method. The nonlinear equations are linearized about the steady equilibrium condition. The equations are those of

$$[M]\ddot{X} + [C]\dot{X} + [K]X = 0 \quad (11)$$

where $[M]$, $[C]$ and $[K]$ are the mass, damping, and stiffness matrices.

For isolated rotor case, the d. o. f. are

$$X = \{\beta, \xi, v\}^T \quad (12)$$

For coupled rotor/body case, the d. o. f. are

$$X = \{\beta, \xi, v, \varphi\}^T \quad (13)$$

The eigenvalues of the Eq. (11) is evaluated to analyse the stability of system. The modal damping is the negative real part of eigenvalue σ . If modal damping is positive, the perturbed motion is stable. The imaginary part of the eigenvalue ω represents not only the modal frequency not also the direction and angular velocity of the whirling motion.

Results and Discussion

Comparison of Theory and Experiment

The analytical model is verified through the comparative study between theoretical results and experimental data. The experiments include the isolated rotor flap/lag stability experiment (Ref. 5) and the coupled rotor-body stability experiment (Ref. 6).

The major rotor properties from Refs. 5-6 are shown in Table 1.

Table 1 Model Rotor Properties

Number of Blades	3	
Rotor radius	31.92 in.	
Blade chord	1.65 in.	
Solidity	0.0493	
Airfoil	NACA23012	
Hinge offset	0.105R	0.111R
	(Ref. 6)	(Ref. 5)
Lock number	7.37	7.54
	(Ref. 6)	(Ref. 5)

The experimental investigation of isolated rotor

stability in hover was conducted in the wind tunnel. The experiment measured the damping and frequency of lead-lag regressive mode (LR) at different blade pitches with rotor speed varying from 100rpm to 1000rpm. In Fig. 2, the frequency and damping of the lead-lag mode predicted data with dynamic inflow is compared with the test data with blade pitch set to zero. The correlation between theory and experiment is excellent. It should be mentioned that the difference between calculation with and without dynamic inflow is negligible in this case because of no aerodynamic and inertial coupling between flap and lead-lag motion. For $\theta_0 = 4^\circ, 6^\circ$ and 8° , the inclusion of dynamic inflow improves the correlation, especially with the L_2 matrix. However for $\Omega > 700$ rpm, the deviation between the theory and the test data is obvious. It increases with increasing blade pitch and rotor speed because of the recirculation in wind tunnel, as analysed in the Ref. 5. Here the case with $\theta_0 = 8^\circ$ is presented in Fig. 3. The deviation in this study is less than that in Ref. 5.

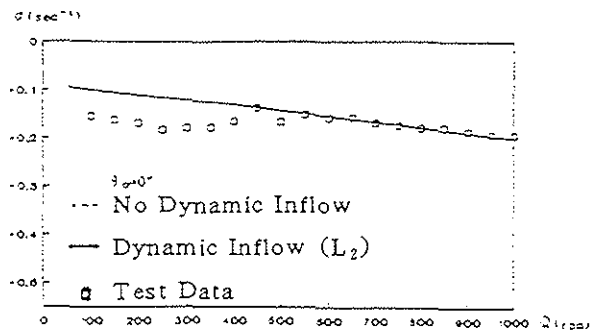
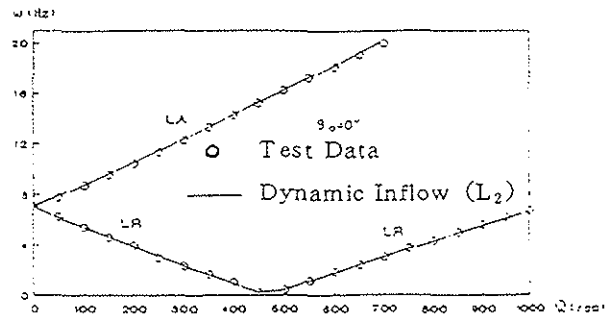


Fig. 2 Comparison of theory and experiment for isolated rotor for frequency and damping of lead-lag mode ($\theta_0 = 0^\circ$).

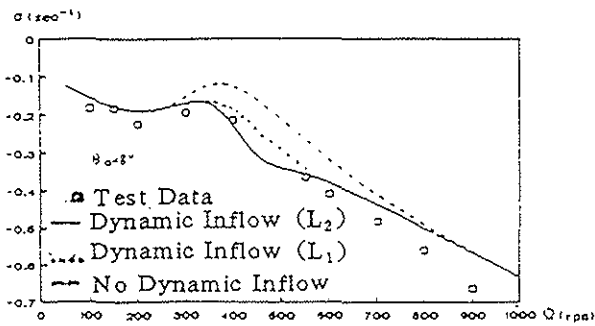


Fig. 3 Comparison of theory and experiment for isolated rotor for the damping of lead-lag regressive mode ($\theta_0 = 8^\circ$).

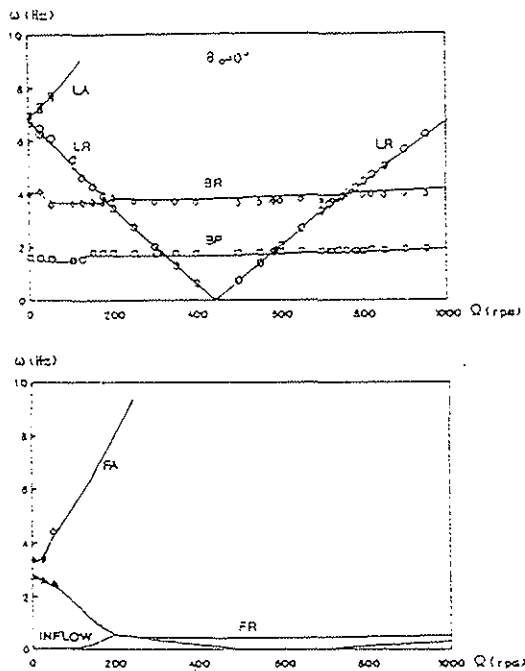


Fig. 4 Comparison of theory and experiment for coupled rotor/body for frequencies ($\theta_0 = 0^\circ$).

The complete test data of coupled rotor-body stability model experiment were provided in Ref. 6. In this study, theory results are compared with the measured modal frequency and damping for cases 1 and 2. Case 1 measured modal damping and frequency with blade pitch set to zero. Damping and frequency of the LR, body pitch mode (BP), and body roll mode (BR) are obtained for rotor speed varying from 0 to 950 rpm. Modal frequencies in

the fixed coordinate are shown in Fig. 4. The theoretical prediction shows good correlation with the measurement. For rotor speeds above 450 rpm, the system is unstable as the LR mode couples with the BP or BR mode.

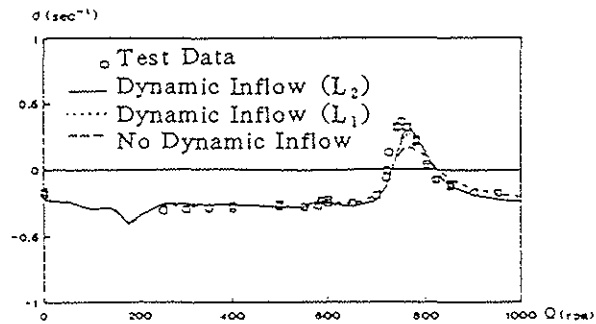


Fig. 5 Comparison of theory and experiment for coupled rotor/body for damping of lead-lag regressive mode ($\theta_0 = 0^\circ$).

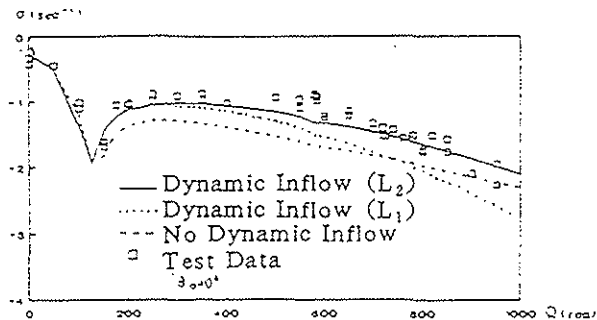


Fig. 6 Comparison of theory and experiment for coupled rotor/body for damping of body pitch mode ($\theta_0 = 0^\circ$).

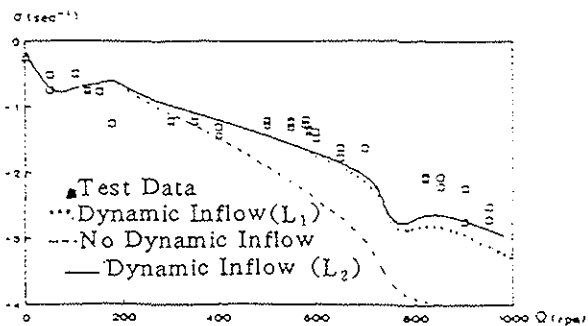


Fig. 7 Comparison of theory and experiment for coupled rotor/body for damping of body roll mode ($\theta_0 = 0^\circ$).

The damping of the LR, BP and BR modes for case 1 is shown in Figs. 5—7. Calculations with dynamic inflow and without dynamic inflow are compared separately. The unstable region (Fig. 5) is centred near the coalescence point of the LR and BR modes, while the damping of BR mode (Fig. 7) has an opposite peak (the experiment did not reveal it).

For rotor speeds near 600rpm where LR mode crosses BP mode, the damping of LR mode has a little decrease. But the LR mode is still stable because of lower rotor speed and higher body pitch structural damping. The damping of BP mode rapidly increases as the LR mode and BP mode become strongly coupled between 100rpm and 150rpm. (Fig. 6)

Compared with the theoretical results without dynamic inflow, the body modal damping is decreased and a better match with the experimental data is provided by taking dynamic inflow into account. However, the damping of LR mode is slightly affected by dynamic inflow.

In the calculation, the two L matrices of dynamic inflow model are compared as shown in Figs. 5—7. It is obvious that the results calculated with the L_2 are better matched with test data than those with the L_1 .

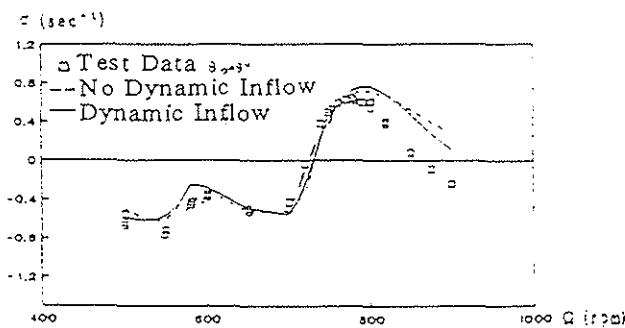


Fig. 8 Comparison of theory and experiment for coupled rotor/body for damping of lead-lag regressive mode ($\theta_0=9^\circ$).

For case 2, the blade pitch angle is set to 9 degrees. Comparison of theory and experiment for the LR modal damping is shown in Fig. 8 as a func-

tion of rotor speed. In this case, the unstable region is wider than the case 1 (Fig. 5), because of the aerodynamic and inertial coupling between lead-lag and flapping motions.

Influence of Dynamic Inflow on Isolated Rotor Flap/Lag Stability

In this study, the effect of dynamic inflow in different conditions is investigated. The L_2 matrix is used in the calculation. The parameters summarized in Table 2 are typical for conventional hingeless rotor helicopters. In the analysis of isolated rotor or rotor / body stability, the most influential parameters are uncoupled dimensionless blade flap and lead-lag natural frequency ($\bar{\omega}_\beta, \bar{\omega}_l$). The variation of $\bar{\omega}_\beta$ and $\bar{\omega}_l$ with rotor speed ratio Ω/Ω_0 is shown in Fig. 9. All parameters are the same as the those used in Ref. 4.

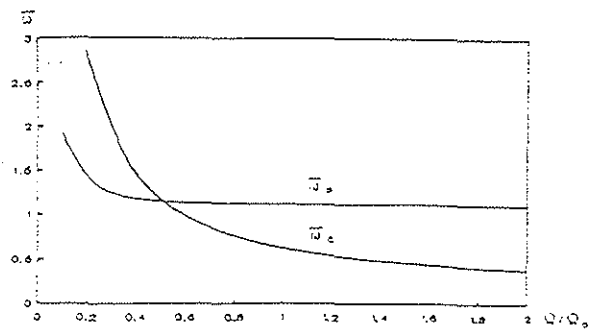


Fig. 9 Variation of $\bar{\omega}_\beta$ and $\bar{\omega}_l$ versus Ω/Ω_0 .

Table 2 Helicopter Parameters in the Analysis

\bar{h}	0.312
σ	0.08218
γ	10
C_l	2π
C_d	0.01
I_b	6.147
δI_h	0.

The variation of real part of the eigenvalue σ with $\bar{\omega}_\beta$ for the isolated rotor at $\theta_0=0.3$ rad and $\bar{\omega}_l=0.8$ is shown in Fig. 10. Comparing the Fig. 10(a)

and (b), it can be found that the damping of lead-lag modes increases with the dynamic inflow taken into account. In order to analyse the influence of inflow mode (DI) on other modes, it is important to identify the DI mode. But it is difficult because the DI mode is highly coupled with flap regressive mode (FR). In Ref. 2, the DI and FR modes were identified only by comparing the participation factors of flap d. o. f. (β) and inflow d. o. f. (v) in the eigenvectors. In the FR mode, the β has a higher participation factor than the v . In the DI mode, the β and the v have almost equal participation factor. But the influence of dynamic inflow on the FR mode identified by this way in Ref. 2 seems to contradict the results in Ref. 3. In this study, the DI and FR modes are identified by comparing the percentage of the v and the β in the eigenvectors since both the v and the β have the "velocity" concept. For example, the percentage of the v and the β corresponding to the modes identified as the DI and FR in Fig. 10(b) are shown in Table 3.

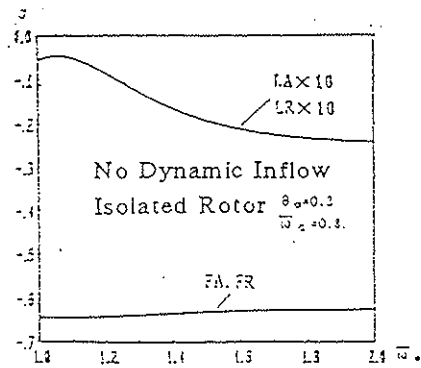
Table 3 Percentage of the v and the β in DI and FR modes

	$\bar{\omega}_p=1$		$\bar{\omega}_p=2$	
	DI	FR	DI	FR
v_c	1.00	-.07	1.00	0.43
v_s	0.11	0.87	0.07	-.56
β_c	0.21	1.00	0.46	0.65
β_s	-.73	0.48	-.13	1.00

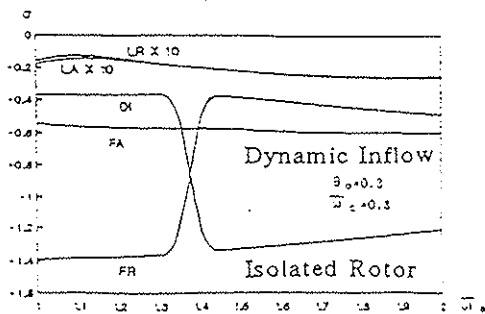
The source of the increase in the lead-lag modal damping with the inclusion of dynamic inflow is investigated through the analysis of the mutual excitation between v and β and between v and ξ , and the analysis of mode shapes. In the LR mode, the aerodynamic lift due to dynamic inflow is out of phase with the blade flapping velocity and the aerodynamic drag due to dynamic inflow is also out of phase with the blade lead-lag velocity. So the work done by inflow on flapping motion and lead-lag motion is negative. It makes the LR mode more stable.

The variation of σ with $\bar{\omega}_t$ at $\theta=0.3$ rad and $\bar{\omega}_s=1.15$ is shown in Fig. 11. Modal damping versus rotor speed ratio Ω/Ω_0 is shown in Fig. 12. The damping of lead-lag modes increases significantly and the system becomes stable with the inclusion of dynamic inflow. For flap advancing mode (FA) and FR mode, the damping decreases due to the positive work done by dynamic inflow on flapping motion. The inflow mode is a heavily damped mode.

In summary, for isolated rotor stability, the major effect of dynamic inflow is to significantly improve the damping of lead-lag mode.



(a)



(b)

Fig. 10 Real part of eigenvalue versus $\bar{\omega}_s$ for isolated rotor with and without dynamic inflow ($\theta_0=0.3$ rad, $\bar{\omega}_t=0.8$).

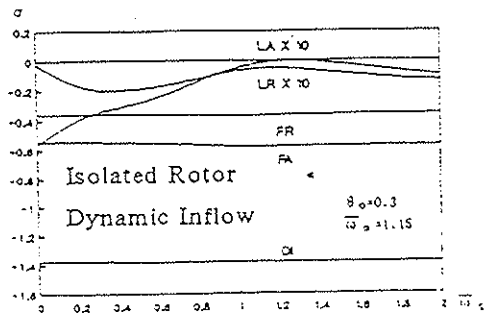
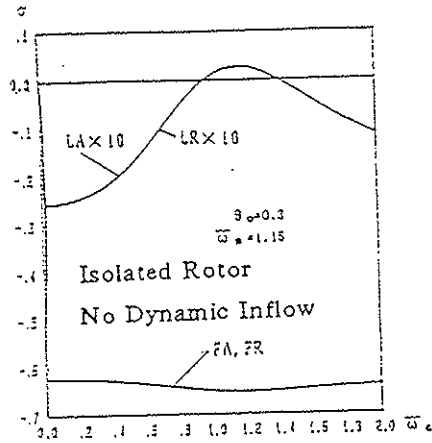


Fig. 11 Real part of eigenvalue versus $\bar{\omega}_1$ for isolated rotor with and without dynamic inflow ($\theta_0 = 0.3$ rad, $\bar{\omega}_b = 1.15$).

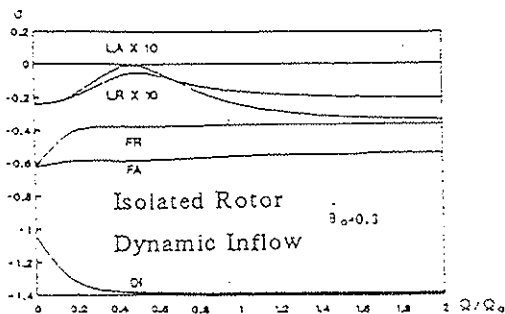
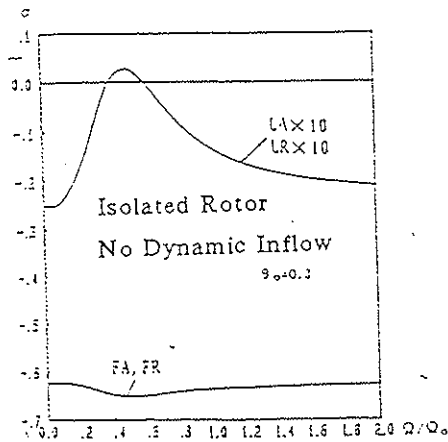


Fig. 12 Real part of eigenvalue versus Ω/Ω_0 for isolated rotor with and without dynamic inflow.

Influence of Dynamic Inflow on Coupled Rotor/Body Stability

For the coupled rotor/body system, besides the LR, LA, FA, FR and DI modes there are gyroscopic mode (GS) and a zero root mode. Here, the calculation with dynamic inflow is compared with that without dynamic inflow in Ref. 4. The variation of eigenvalue with $\bar{\omega}_b$ at $\theta_0 = 0.3$ rad and $\bar{\omega}_1 = 0.8$ is shown in Fig. 13. The mode with low modal frequency and heavy modal damping is DI mode. For the modal frequency, the effect of dynamic inflow is slight. Although the damping of LA becomes positive (negative eigenvalue) with the inclusion of dynamic inflow, the damping of the LR keeps almost unchanged and LR is still unstable. Now there are three sources of instability in the LR mode: positive mutual excitation between ξ and β , between ξ and ψ and between λ and ξ .

For FA mode and FR, the modal damping decreases with dynamic inflow.

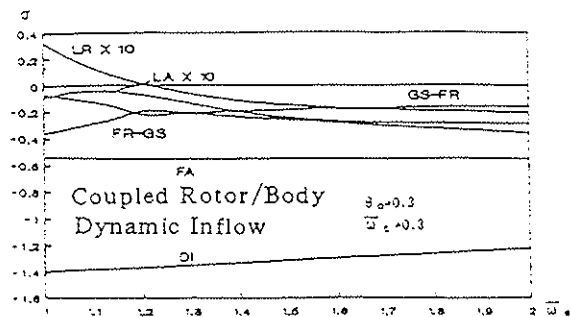
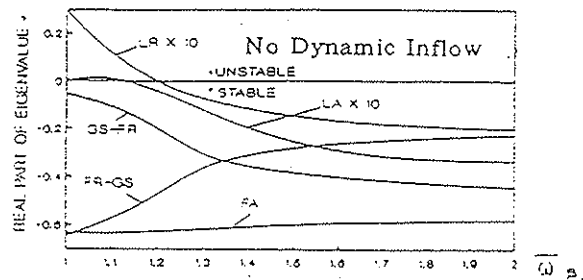


Fig. 13 Real part of eigenvalue versus $\bar{\omega}_b$ for coupled rotor/body with and without dynamic inflow ($\theta_0 = 0.3$ rad, $\bar{\omega}_1 = 0.8$).

Modal damping of the LR and LA modes versus $\bar{\omega}_1$ at different collective pitch is shown in Fig. 14.

The variation of σ for LA and LR modes versus rotor speed ratio Ω/Ω_0 at $\theta_0 = 0, 0.13, 0.3$ rad is shown in Fig. 15. Compared with the case of no dynamic inflow, the damping of the LA mode is increased significantly by taking dynamic inflow into account. The effect of dynamic inflow increases with the increase of the collective pitch.

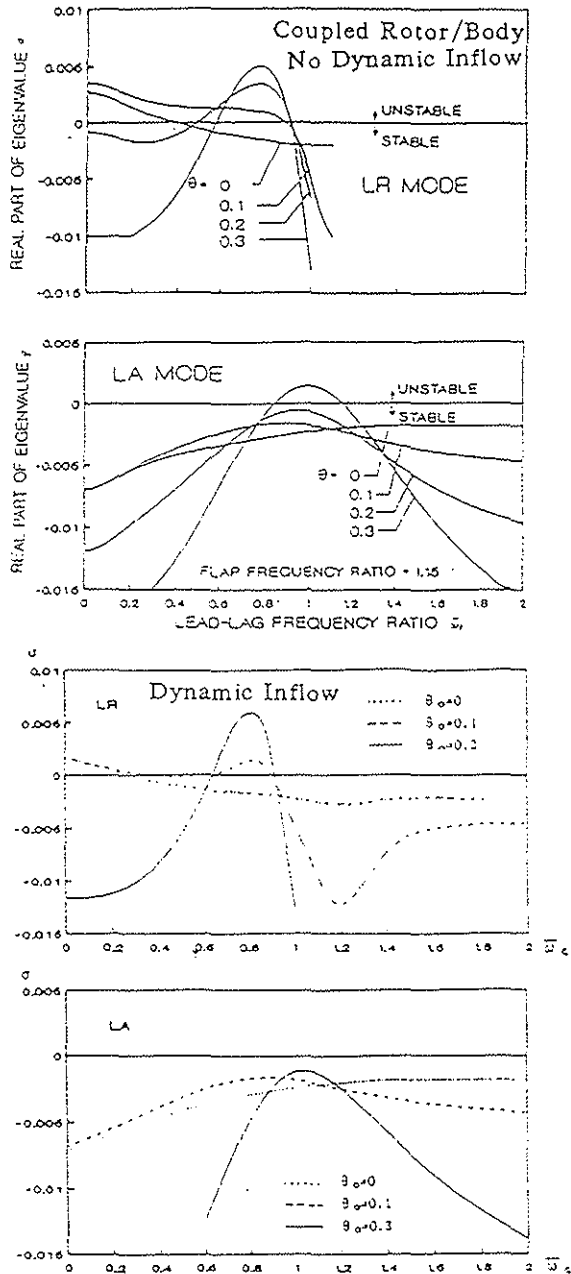


Fig. 14 Real part of eigenvalue of the LR and LA modes versus $\bar{\omega}_1$ for coupled rotor/body with and without dynamic inflow ($\bar{\omega}_2 = 1.15$).

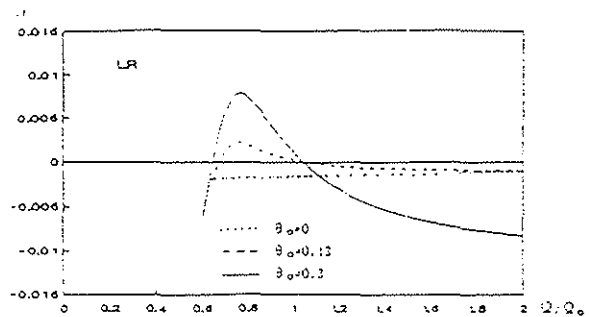
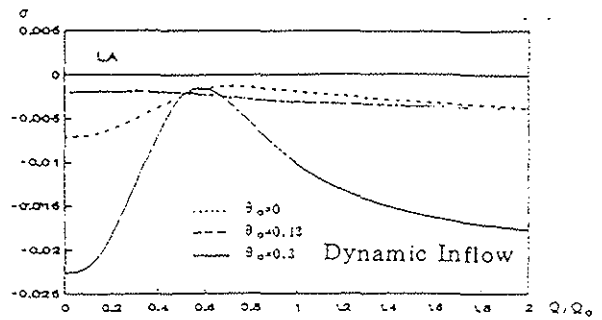
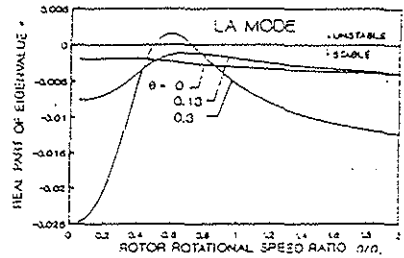
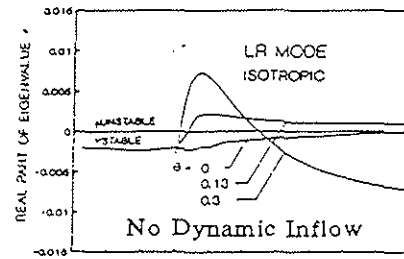


Fig. 15 Real part of eigenvalue of the LR and LA modes versus Ω/Ω_0 for coupled rotor/body with and without dynamic inflow.

Conclusions

1. The correlation between theoretical predictions taking dynamic inflow into account and experimental data is excellent.
2. The effect of dynamic inflow on the modal frequency is slight.
3. For the analysis of isolated rotor flap/lag sta-

bility, the damping of lead-lag modes increases with the inclusion of dynamic inflow.

4. For the analysis of coupled rotor/body stability, the damping of lead-lag advancing mode increases with the inclusion of dynamic inflow, and the damping of lead-lag regressive mode is affected by dynamic inflow slightly.

5. The damping of the flap modes decreases with the inclusion of dynamic inflow.

6. The source of the increase of modal damping with dynamic inflow is the negative work done by inflow on other d. o. f. . And the source of the decrease of modal damping with dynamic inflow is the positive work done by inflow on other d. o. f. .

7. The theoretical results calculated with the L_2 matrix of dynamic inflow model are better matched with test data than those with the L_1 matrix.

Reference

- 1 X. Zhang and J. Bao. Investigation of Dynamic Inflow's Influence on Rotor Control Derivatives. Joint Proceedings on Aeronautics & Astronautics, ISBN 7-80046-602/V · 139, China Aviation Industry Press, May, 1993. (in English)
- 2 P. P. Friedmann and C. Venkatesan. Influence of Various Unsteady Aerodynamic Models on the Aeromechanical Stability of a Helicopter in Ground Resonance. 2nd Decennial Specialists' Meeting on Rotorcraft Dynamics, NASA Ames Research Center, Moffett Field, Calif., June 1983.
- 3 J. M. Wang, J. Jang and I. Chopra. Air Resonance Stability of Hingeless Rotors in Forward Flight. *Vertica* Vol. 14, No. 2, 1990.
- 4 X. Zhang. Investigation of Helicopter Air Resonance in Hover by Complex Coordinates and Mutual Excitation Analysis. *Journal of the American Helicopter Society*, Vol. 38, No. 2, 1993.
- 5 G. H. Gaonkar. An experimental and analytical investigation of isolated rotor flap-lag stability in forward flight. Proceedings of eleventh European rotorcraft forum, London, 1985
- 6 W. G. Boušman. A comparison of theory and experiment for coupled rotor-body stability of a hingeless rotor model in hover. NASA CP-10007, 1988.
- 7 D. M. Pitt and D. A. Peters. Theoretical Prediction of Dynamic Inflow Derivatives. Proceedings of 6th European Rotorcraft and Powered Lift Aircraft Forum, Paper No. 47, Bristol, England, 1980.
- 8 W. Johnson. *Helicopter Theory*, Princeton University Press, 1980.